JOURNAL OF SPACECRAFT AND ROCKETS
Vol. 46, No. 1, January–February 2009

Influence of Shock Waves on Supersonic Film Cooling

Wei Peng and Pei-Xue Jiang*
Tsinghua University, 100084 Beijing, People's Republic of China

DOI: 10.2514/1.38458

Supersonic film cooling with and without induced shock waves was investigated numerically. The computations used a freestream Mach number of 3.13 and tangential-slot injection-cooling-stream Mach numbers of 1.3 and 1.8. Parameters investigated included shock wave intensity and coolant properties (nitrogen, methane, and helium). The results indicate that the adiabatic effectiveness is reduced by the impinging oblique shock wave because the shock wave reduces the local Mach number in the coolant layer, which increases the adiabatic-wall temperature. In addition, the oblique shock wave enhances the mixing of the cooling stream with the freestream, especially for stronger shock waves or lighter-gas coolants, which also increases the adiabatic-wall temperature. For the same injection-cooling-stream Mach number, the effects of the oblique shock wave are stronger in helium; however, helium had a higher adiabatic effectiveness than methane and nitrogen, even though the helium mass flow rate was lower than that of either methane or nitrogen. The adiabatic effectiveness is reduced much more by the 10 deg shock waves than by either the 7 or 4 deg shock waves.

Nomenclature

c_i	=	mass concentration, kg/m^3
c_p	=	specific heat capacity, J/kg · K
D_{im}	=	diffusion coefficient, m^2/s
k	=	turbulent kinetic energy, m^2/s^2
Ma	=	Mach number
P	=	pressure, Pa
Pr	=	Prandtl number
r	=	recovery factor
T	=	temperature, K
T_{aw}	=	local adiabatic-wall temperature, K
T_c	=	cooling-stream-flow static temperature, K
T_{oe}	=	total temperature at the edge of the boundary layer, K
T_{rc}	=	cooling-stream-flow recovery temperature, K
$T_{r\infty}$	=	freestream flow recovery temperature, K
T_∞	=	freestream flow static temperature, K
x	=	distance from the slot along the surface, m
γ	=	gas specific heat ratio
η	=	adiabatic effectiveness
μ	=	dynamic viscosity, Pa · s
ρ	=	density, kg/m^3

Subscripts

ad	=	adiabatic
c	=	cooling stream
r	=	recovery condition
∞	=	freestream

I. Introduction

FILM cooling is the introduction of a secondary fluid (coolant or injected fluid) at one or more discrete locations along a surface exposed to a high-temperature environment to protect that surface not only in the immediate region of injection, but also in the downstream region [1]. Film cooling is widely used in gas turbines, blades, combustion-chamber walls, and nozzles. Moreover, film cooling has also been considered as a means to protect both the external wall and the internal combustor duct of supersonic or hypersonic vehicles.

The literature on film cooling is very extensive. The majority of these studies have focused on subsonic film cooling. In supersonic flows, shock waves can cause phenomena that do not occur in subsonic flows, such as breaking of the coolant boundary and altering of the pressure distribution. Therefore, supersonic film cooling must account for the effect of oblique shock waves.

Experimental studies [2–7] reported on supersonic film cooling with shock waves. In an early study of supersonic film cooling, Alzner and Zakkay [2] investigated the effect of an impinging shock wave on the local flowfield structure and the film-cooling effectiveness. Their experimental results showed a significant effect of the shock wave on film cooling. However, Ledford and Stollery [3] found that the shock wave had little effect on film cooling. The different results may be due to the different shock strengths in their studies. Juhany and Hunt [4] also considered the effect of the shock wave in supersonic film cooling and showed that the impingement of an incident shock decreases the film-cooling effectiveness, due to a decrease in the local Mach number. However, in their experiments, the shock impingement was located well downstream of the injection nozzle, and so their conclusion cannot be directly applied to situations in which the shock impingement occurs much closer to the nozzle. Experimental research by Kanda et al. [5,6] showed that a weak shock wave did not reduce the film-cooling effectiveness, whereas a strong shock wave reduced the film-cooling effectiveness in a restricted region. They also found that the reduced effectiveness was mainly due to the increased adiabatic temperature caused by the reduced local Mach number. The shock impingement in their experiments was much closer to the nozzle, but they used argon as the coolant and did not consider lighter gases such as helium or hydrogen. Moreover, the shock wave generators in their experiments had angles of 6, 7, and 8 deg, and so they did not consider much stronger shock waves; thus, their conclusions for the shock wave effect on the film-cooling effectiveness might be unsuitable for cases with stronger shock waves and lighter-gas coolants.

This paper considers supersonic film cooling of a flat surface with an impinging oblique shock wave. The freestream was assumed to be air; the coolants were nitrogen, methane, and helium; and the three shock wave generators had angles of 10, 7, and 4 deg.

II. Problem Description and Computational Model

A. Problem Description

The present study focuses on the injection of a cooling stream through a rearward-facing slot parallel to the stream flow on a flat surface. A wedge shock generator was used to produce the shock wave. The supersonic flow impinges upon the shock generator to

Received 15 May 2008; accepted for publication 15 July 2008.

*Key Laboratory for Thermal Science and Power Engineering of the Ministry of Education, Department of Thermal Engineering; Jiangpx@tsinghua.edu.cn.

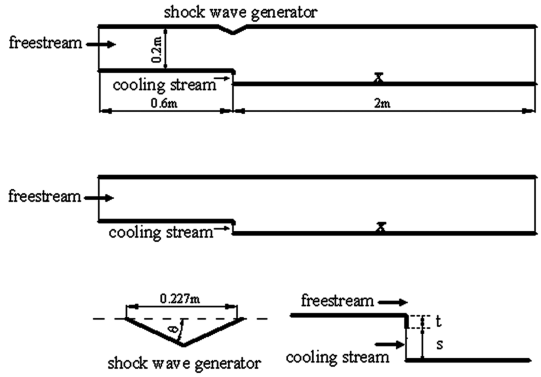

Fig. 1 Sketches of the physical models.

produce an oblique shock wave. Figure 1 shows the geometry with the shock wave generator. The flows were analyzed with wedge angles θ of 10, 7, and 4 deg. The shock wave generator base was 0.227 m long. The whole channel was 2.6 m long with 0.6 m before the cooling-stream slot. The stream flow inlet was 0.2 m high and the cooling-stream slot was 8 mm high, with the whole step height being 8.4 mm high, so that in Fig. 1, $s = 8$ mm and $t = 0.4$ mm. The same geometry without the shock wave generator was also used to study the flow without the shock wave.

B. Numerical Method

The simulations were performed using the CFD software package FLUENT (version 6.3.26), which uses the Favre-averaged equations to analyze the fluid flow for the continuity, momentum, energy, and mass transport equations. Turbulence closure was achieved using the shear-stress transport (SST) κ-ω model. The SST κ-ω model, so named because the definition of the turbulent viscosity is modified to account for the transport of the principal turbulent shear stress, gradually changes from the standard κ-ω model in the inner region of the boundary layer to the transformed κ-ε model (in a κ-ω formulation) in the outer part of the boundary layer.

The general forms of the governing equations for this problem are

$$\nabla \cdot (\rho U \phi) = \nabla \cdot (\Gamma_\phi \nabla \phi) + S \tag{1}$$

The variables are defined in Table 1 for each equation. S_Φ represents the viscous dissipation terms, which describe the thermal energy created by the viscous shear; G_k represents the generation of turbulence kinetic energy due to the mean velocity gradients; G_ω represents the generation of ω; Y_k and Y_ω represent the dissipation of k and ω due to turbulence; D_ω represents the cross-diffusion term; D_{im} represents the diffusion coefficient for species i; and Sc_t represents the turbulent Schmidt number.

The advection terms in the momentum, energy, mass transport, turbulent kinetic energy, and specific dissipation equations were discretized using the second-order upwind algorithm. The iterations were continued until all the relative residuals were less than 10^{-3}.

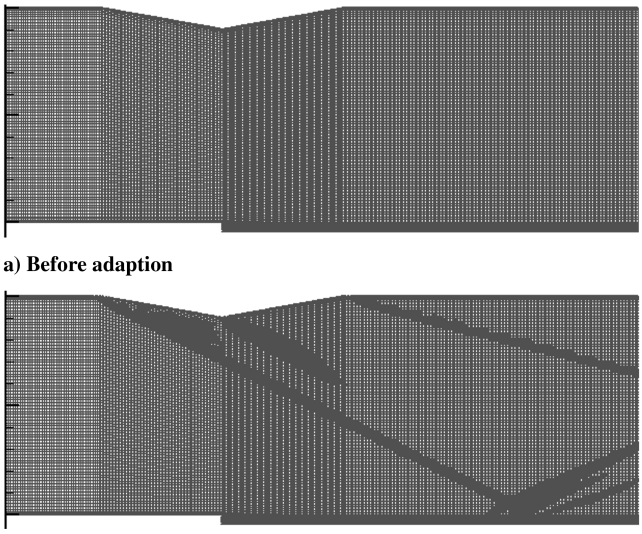

a) Before adaption

b) After adaption

Fig. 2 Mesh along the surface with the oblique shock model.

C. Boundary Conditions

The freestream and cooling-stream boundary conditions are listed in Table 2. The freestream inlet conditions were kept constant for all cases. The other walls were assumed to be insulated with the no-slip boundary condition. The outlet was specified as a pressure outlet.

D. Mesh

Grid independence studies resulted in meshes having about 170,000 elements for each case. To catch the shock wave more exactly, the mesh adaption function in FLUENT was used to refine the mesh around the shock wave, with about 180,000 elements after adaption. Figure 2 shows the meshes with the shock wave generator before and after mesh adaption.

III. Results and Discussion

A. Validation of the Computational Procedure

The numerical approach was validated, including whether the turbulence model is suitable for supersonic flows, by comparing the results for supersonic film cooling along a flat plate with the experimental results of Juhany et al. [7] The results in Fig. 3 show good agreement between the simulations and the experimental data, which used air and helium as coolants.

Table 1 Definitions used in the governing equations

	ϕ	Γ_ϕ	S
Continuity equation	1	0	0
Momentum equation	u	$\mu + \mu_t$	$-(\partial p_{\text{eff}}/\partial x) + (\partial/\partial x)[(\mu + \mu_t)(\partial u/\partial x)] + (\partial/\partial y)[(\mu + \mu_t)(\partial v/\partial x)]$
	v	$\mu + \mu_t$	$-(\partial p_{\text{eff}}/\partial y) + (\partial/\partial x)[(\mu + \mu_t)(\partial u/\partial y)] + (\partial/\partial y)[(\mu + \mu_t)(\partial v/\partial y)]$
Energy equation	T	$\mu/Pr + \mu_t/\sigma_t$	S_Φ
Mass transport equations	c_i	$D_{\text{im}}/\mu_t/Sc_t$	0
Turbulence transport	k	$\mu + \mu_t/\sigma_k$	G_k-Y_k
Equations	ω	$\mu + \mu_t/\sigma_\omega$	G_ω-$Y_\omega + D_\omega$

Table 2 Inlet boundary conditions

Nomenclature	Ma	Inlet static pressure, kPa	Inlet total temperature, K
Freestream	3.13	61	1400
Cooling stream	1.3	61	300
	1.8	61	300

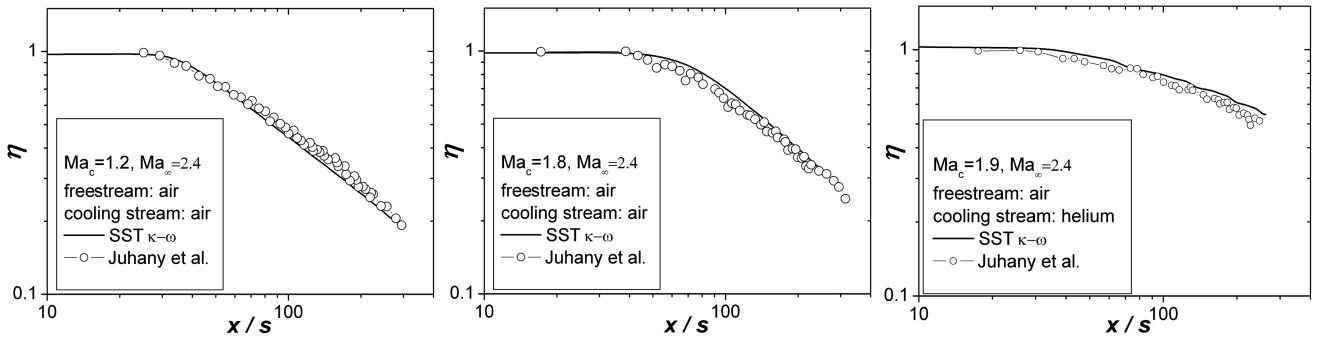

Fig. 3 Comparison of the numerical results with the experimental data of Juhany et al. [7].

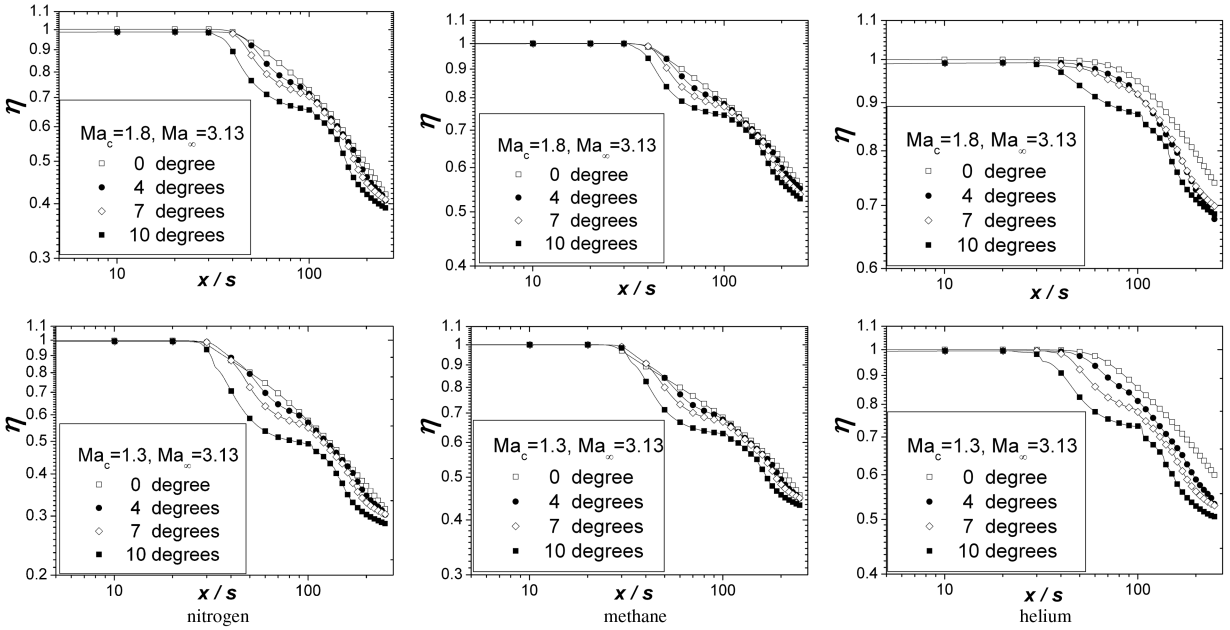

Fig. 4 Adiabatic effectiveness for three coolants with and without shock waves.

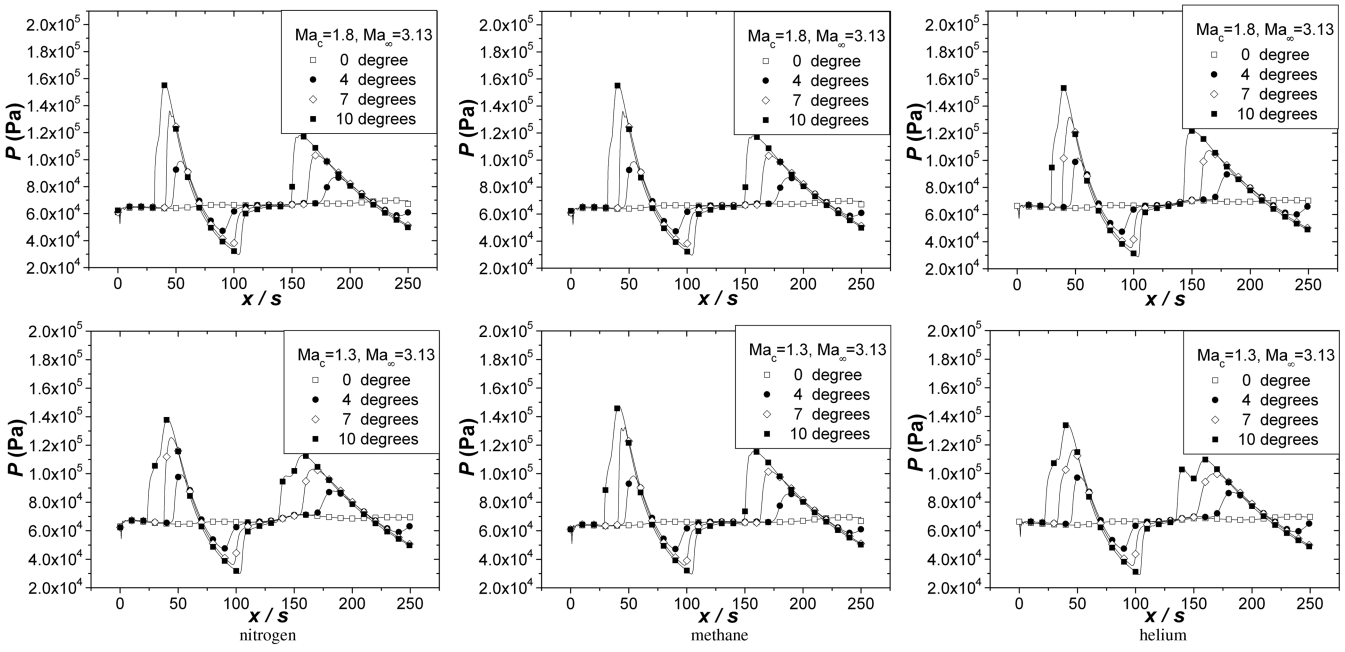

Fig. 5 Static pressure on the wall with and without the shock wave.

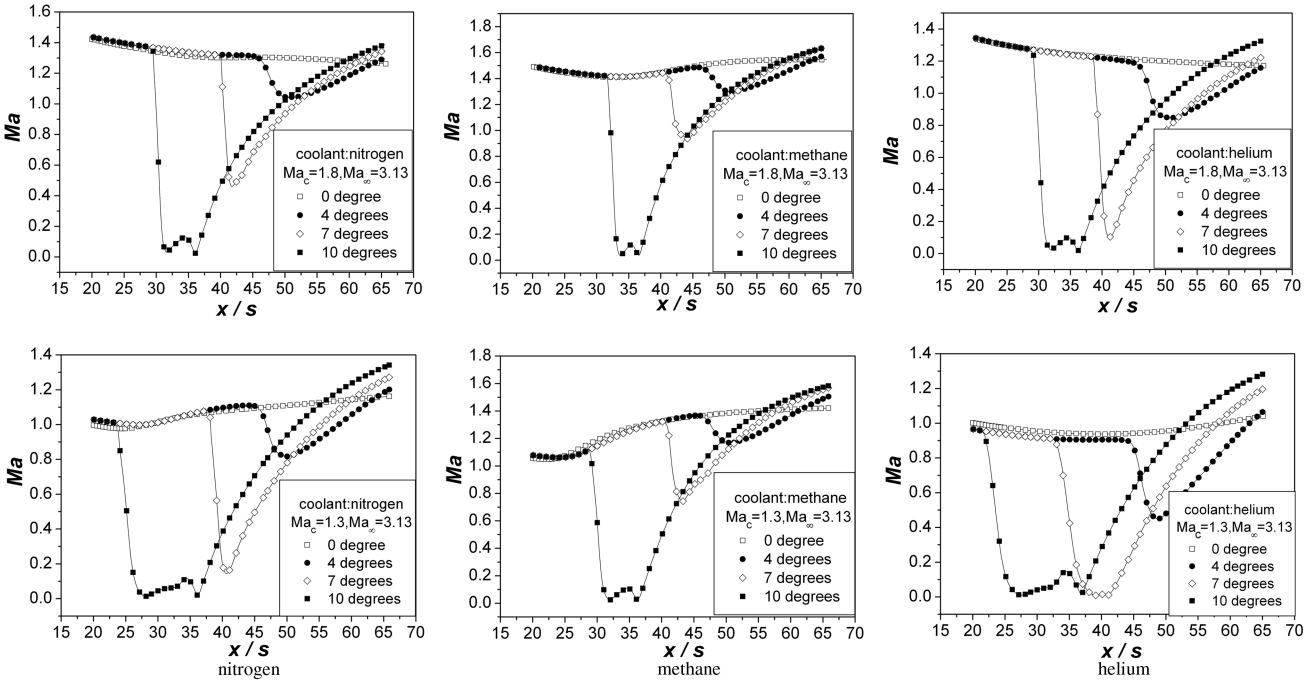

Fig. 6 Mach number distributions in the shock wave interaction region (1 mm above the wall).

In supersonic film cooling, the adiabatic effectiveness is defined as

$$\eta = \frac{T_{r\infty} - T_{\mathrm{aw}}}{T_{r\infty} - T_{\mathrm{rc}}} \tag{2}$$

where $T_{r\infty}$ is the freestream recovery temperature, T_{rc} is the cooling-stream recovery temperature defined as

$$T_{r\infty} = T_{\infty}\left(1 + r\frac{\gamma - 1}{2}Ma_{\infty}^2\right) \tag{3}$$

$$T_{\mathrm{rc}} = T_c\left(1 + r\frac{\gamma - 1}{2}Ma_c^2\right) \tag{4}$$

and T_{aw} is the adiabatic-wall temperature expressed as

$$T_{\mathrm{aw}} = T_{\mathrm{oe}}\left[r + \frac{1 - r}{1 + \frac{\gamma-1}{2}Ma^2}\right] \tag{5}$$

B. Effects of the Oblique Shock Wave

The flowfields were analyzed with air as the freestream and with nitrogen, methane, and helium as coolants, with and without the oblique shock wave. Figure 4 shows the adiabatic effectiveness for these three coolants. The results show that the adiabatic effectiveness is reduced by the impinging oblique shock wave, with the 10 deg shock wave generator having the largest effect.

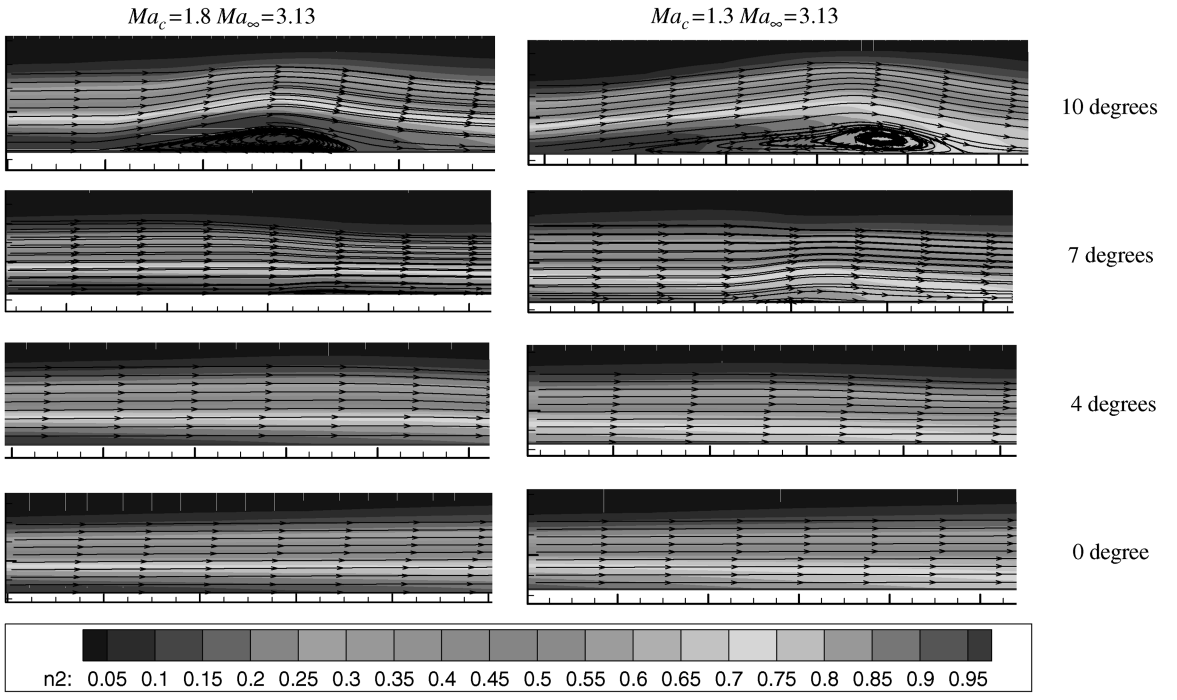

Fig. 7 Nitrogen mass-fraction contours and velocity distributions in the shock wave interaction zone.

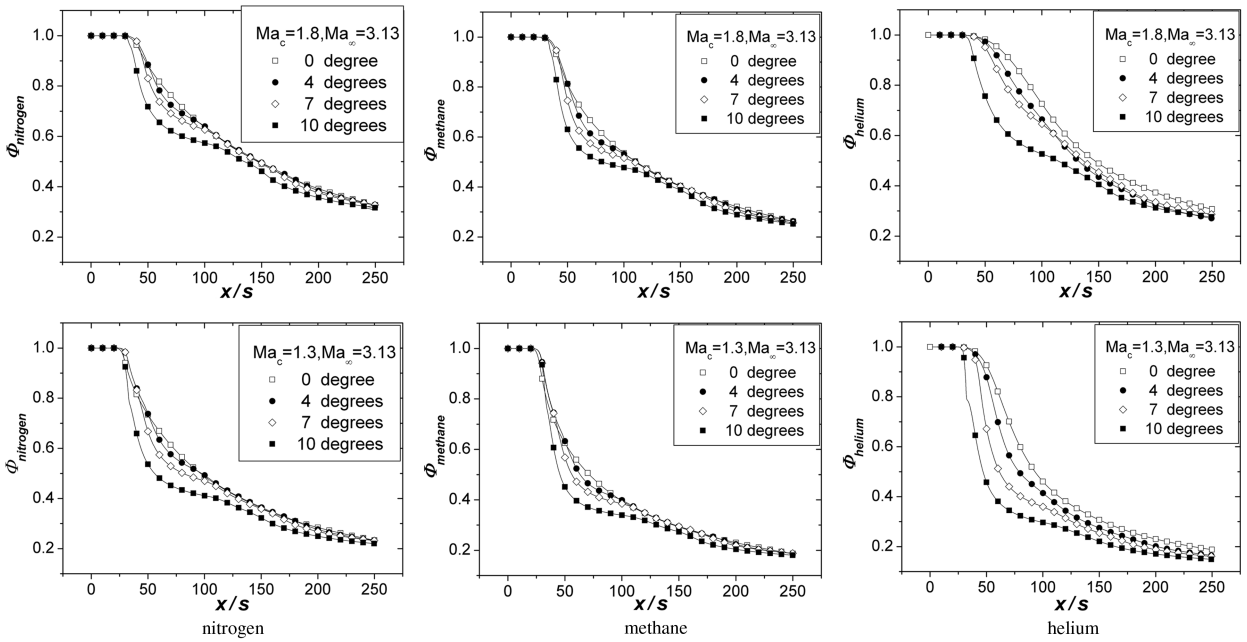

Fig. 8 Coolant mass-fraction distributions near the wall.

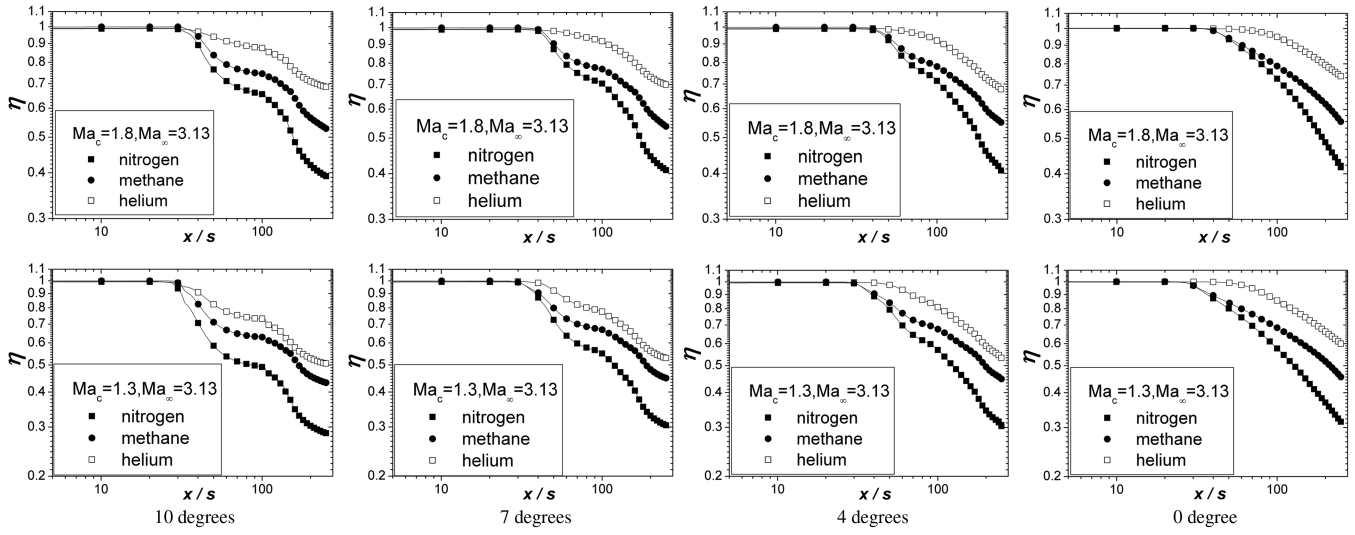

Fig. 9 Adiabatic-effectiveness distributions for the three coolants.

The effectiveness is reduced by increases of the adiabatic-wall temperature due to decreases of the local Mach number in the shock wave interaction region. Figure 5 shows the static pressure on the wall protected by the cooling stream with and without the oblique shock wave. When the oblique shock wave interferes with the cooling-stream boundary, the coolant static pressure increases and the Mach number of the coolant layer decreases, as shown in Fig. 6.

When the Mach number of the coolant layer decreases for the same T_{oe}, T_{aw} increases, which reduces the adiabatic effectiveness. As the shock wave becomes stronger, the Mach number of the coolant layer further decreases, T_{aw} then increases more, and the adiabatic effectiveness becomes lower. In Fig. 6, the local Mach number in the shock wave interaction region is lowest for the 10 deg shock wave generator; thus, the adiabatic effectiveness in Fig. 4 is reduced the most by the 10 deg shock wave generator.

The other reason the adiabatic effectiveness is reduced is the increased mixing of the freestream and the cooling stream by the impinging oblique shock wave. With film cooling, the mixing of the freestream and the cooling stream reduces the adiabatic

Table 3 Coolant mass flow rates

	Mass flow rate, kg/s	
Coolant	$Ma_c = 1.3$	$Ma_c = 1.8$
Nitrogen	2.9075	4.4568
Methane	2.1165	3.2205
Helium	1.2972	2.0704

Table 4 Heat capacities of the three coolant streams

	Heat capacities, $J \cdot s^{-1} \cdot K^{-1}$	
Coolant	$Ma_c = 1.3$	$Ma_c = 1.8$
Nitrogen	3022.70	4648.44
Methane	5291.25	8051.25
Helium	6736.36	10751.59

Table 5 Coolant transport properties

Coolant	P, atm	Ma_c	T_{oc}	T, K	M_A	M_B	d_A, Å	d_B, Å	ε_A/k_1, K	ε_B/k_1, K	Ω_{AB}	D_{AB}, cm^2 s^{-1}
Nitrogen	0.602	1.3	300	224	28.02	28.97	3.681	3.617	91.5	97.0	1.019	0.2020
Methane	0.602	1.3	300	235	16.04	28.97	3.758	3.617	148.6	97.0	1.087	0.2342
Helium	0.602	1.3	300	192	4.00	28.97	2.556	3.617	10.2	97.0	0.8091	0.5681
Nitrogen	0.602	1.8	300	182	28.02	28.97	3.681	3.617	91.5	97.0	1.092	0.1381
Methane	0.602	1.8	300	196	16.04	28.97	3.758	3.617	148.6	97.0	1.160	0.1672
Helium	0.602	1.8	300	144	4.00	28.97	2.556	3.617	10.2	97.0	0.8536	0.3498

effectiveness. Figure 7 shows coolant mass-fraction contours and the velocity distributions in the shock wave interaction zone for the nitrogen coolant.

With the 10 deg shock wave generator, the shock wave is stronger and the coolant layer becomes thicker in the shock wave interaction region, which indicates that the flow is restricted in the boundary layer, resulting in increased mixing of the freestream and the cooling stream. Moreover, there is a distinct vortex in the coolant layer, which will also increase the mixing of the main flow and the cooling stream. With the 7 and 4 deg shock wave generators, the shock waves are not as strong as with the 10 deg shock wave generator, and so the flow in the coolant layer does not change as much as with the 10 deg shock wave generator. Similar phenomena occurred with the methane and helium coolants.

The methane and helium mass-fraction distributions near the wall are shown in Fig. 8, which shows that the impinging oblique shock wave reduces the coolant mass fractions. With the 4 and 7 deg shock wave generators, the nitrogen and methane mass-fraction reductions occur mainly in the shock wave interaction region, which corresponds with the reduced adiabatic effectiveness shown in Fig. 4. With the 10 deg shock wave generator, the nitrogen and methane mass fractions are reduced not only in the shock wave interaction region, but also downstream, with the adiabatic effectiveness in Fig. 4 showing similar trends. These results indicate that the stronger shock wave creates more mixing. With helium, the helium mass fraction is reduced both in the shock wave interaction region and downstream, even with the 4 and 7 deg shock wave generators, with the effects more pronounced with the 10 deg shock wave generator. Thus, the mixing enhancement by the shock wave is stronger with helium than with methane or nitrogen.

C. Effects of Coolant Properties

Figure 9 shows the influences of the coolant on the adiabatic effectiveness. For the same injection-cooling-stream Mach number, helium has the highest adiabatic effectiveness with or without the oblique shock wave, with methane having the next-highest effectiveness and nitrogen having the lowest effectiveness. For the same injection-cooling-stream Mach number, the mass flow rate of nitrogen is larger than that of methane and helium, as shown in Table 3.

Helium has the best cooling capability because the specific heat of helium is higher than that of the other coolants. Even though the nitrogen mass flow rate is the highest, the nitrogen specific heat is the lowest, with $c_{p\,\text{nitrogen}} < c_{p\,\text{methane}} < c_{p\,\text{helium}}$, as shown in Table 4, in which the specific heat of the coolant is based on the injection-cooling-stream temperature. Thus, helium has the best cooling performance for the same injection-cooling-stream Mach number.

Figures 4 and 8 show that the shock wave has the largest effect on the helium coolant because the helium diffuses more rapidly than the methane or the nitrogen, as can be shown by the binary diffusion coefficients D_{AB}. If a species of molecular weight M_A is mixed with another species of molecular weight M_B at pressure P and temperature T, then D_{AB} can be defined as [8,9]

$$D_{AB} = 0.00188 \frac{\sqrt{T^3[(1/M_A) + (1/M_B)]}}{P d_{AB}^2 \Omega_{AB}} \tag{6}$$

where D_{AB} has units of cm^2 s^{-1}, T is in Kelvin, P is in atmospheres, d_{AB} is in angstroms and can be reasonably approximated by

$$d_{AB} = \tfrac{1}{2}(d_A + d_B) \tag{7}$$

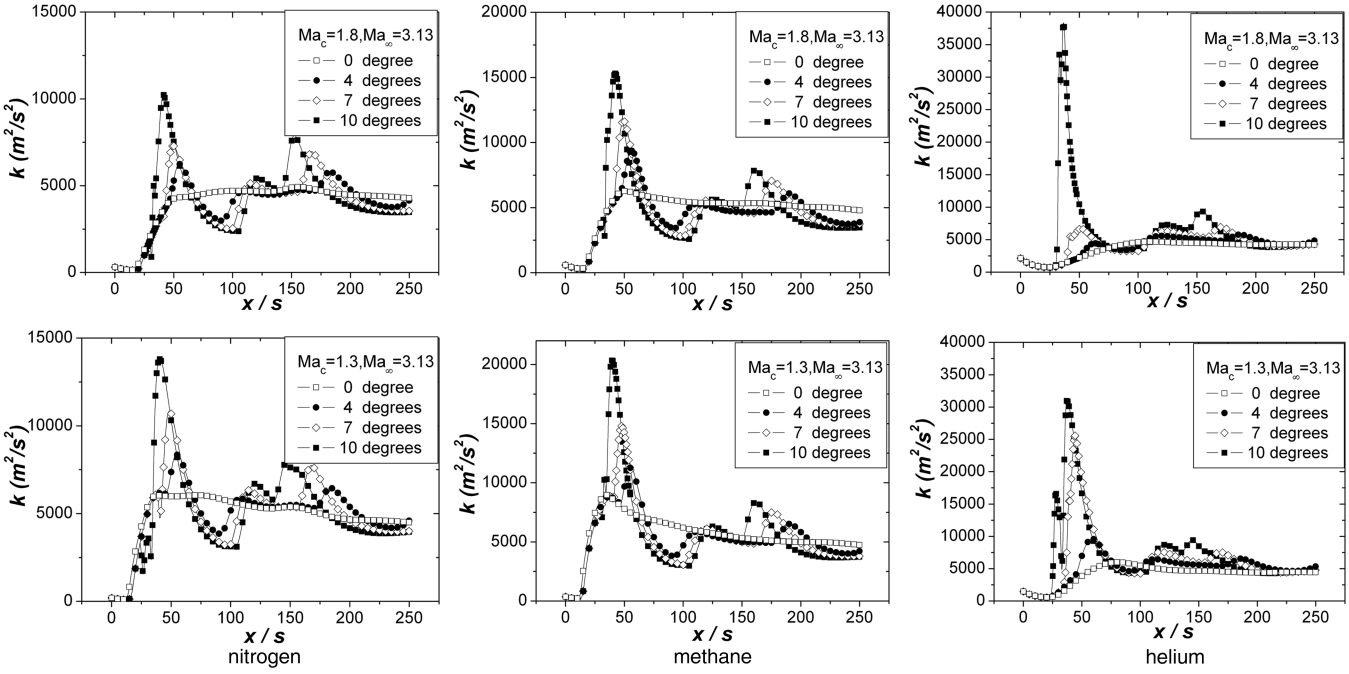

Fig. 10 Turbulent kinetic energies in the boundary layer (4 mm above the wall).

and Ω_{AB} is the collision integral parameter that is a function of $k_1 T/\varepsilon_{AB}$, with k_1 being the Boltzmann constant and $\varepsilon_{AB} = (\varepsilon_A \varepsilon_B)^{1/2}$, where ε_A and ε_B are the characteristic energy interaction parameters for the two species. Table 5 lists the transport properties of the coolant gases.

The binary diffusion coefficient of helium is the largest, which indicates that helium diffuses faster than methane or nitrogen. Nitrogen and methane have similar diffusion coefficients and so the coolant mass-fraction trends for nitrogen and methane are similar. For the same pressure and temperature, with the same species B being air, the binary diffusion coefficient D_{AB} is mainly a function of the molecular weights of species A, which indicates that lighter gases such as helium have higher D_{AB} than heavier gases.

The turbulent kinetic energies in the boundary layer with and without the impinging shock wave are shown in Fig. 10. The turbulent kinetic energy, which represents the interaction intensity between the freestream flow and the cooling stream, is higher in the shock wave interaction region. Thus, stronger shock waves result in higher turbulent kinetic energies, which also means that the mixing of the freestream and the cooling stream is stronger with the stronger shock wave. With these three coolants, the turbulent kinetic energy in the helium boundary layer increases more sharply than for the other two coolants, with methane more influenced by the shock wave than nitrogen. Thus, the turbulent intensity distributions show that the shock wave has a stronger effect on the lighter gas than on the heavier gas.

IV. Conclusions

The analysis of the effect of the impinging oblique shock wave on the supersonic film cooling has shown the following:

1) The oblique shock wave reduces the adiabatic effectiveness because the shock wave increases the static pressure on the wall, which reduces the local Mach number in the coolant layer and the adiabatic effectiveness. The impinging shock wave also enhances the mixing of the freestream and the cooling stream, especially with stronger shock waves or lighter-gas coolants.

2) The 10 deg shock wave generator has a stronger effect on the coolants than the 4 and 7 deg shock wave generators.

3) Helium is more easily affected by the shock wave than methane or nitrogen, because helium diffuses faster than methane or nitrogen. In addition, the shock wave has a stronger effect on lighter gases than on heavier gases.

Acknowledgments

This project was supported by the key project fund from the National Natural Science Foundation of China (no. 50736003) and the National Basic Research Program (973 program) (no. 2007CB210107).

References

[1] Goldstein, R. J., "Film Cooling," *Advances in Heat Transfer*, Vol. 7, 1971, pp. 321–379.

[2] Alzner, E., and Zakkay, V., "Turbulent Boundary Layer Shock Interaction with and Without Injection," *AIAA Journal*, Vol. 9, No. 9, 1971, pp. 1769–1776. doi:10.2514/3.49979

[3] Ledford, O. C., and Stollery, J. L., "Film Cooling of Hypersonic Inserts," Imperial College, Rept. 72-15, London, July 1972.

[4] Juhany, K. A., and Hunt, M. L., "Flowfield Measurements in Supersonic Film Cooling Including the Effect of Shock-Wave Interaction," *AIAA Journal*, Vol. 32, No. 3, 1994, pp. 578–585. doi:10.2514/3.12024

[5] Kanda, T., Ono, F., and Saito, T., "Experimental Studies of Supersonic Film Cooling with Shock Wave Interaction," AIAA Paper 96-2663, July 1996.

[6] Kanda, T., and Ono, F., "Experimental Studies of Supersonic Film Cooling with Shock Wave Interaction 2," *Journal of Thermophysics and Heat Transfer*, Vol. 11, No. 4, 1997, pp. 590–593. doi:10.2514/2.6286

[7] Juhany, K. A., Hunt, M. L., and Sivo, J. M., "Influence of Injectant Mach Number and Temperature on Supersonic Film Cooling," *Journal of Thermophysics and Heat Transfer*, Vol. 8, No. 1, 1994, pp. 59–67. doi:10.2514/3.501

[8] Anderson, J. D., Jr., "Hypersonic and High Temperature Gas Dynamics," *Aeronautical and Aerospace Engineering*, McGraw–Hill, New York, 1989, pp. 596–600.

[9] Sahoo, N., Kulkarni, V., Saravanan, S., Jagadeesh, G., and Reddy, K. P. J., "Film Cooling Effectiveness on a Large Angle Blunt Cone Flying at Hypersonic Speed," *Physics of Fluids*, Vol. 17, No. 3, 2005, Paper 036102. doi:10.1063/1.1862261

G. Palmer
Associate Editor